ACS APPLIED MATERIALS & INTERFACES

Research Article

www.acsami.org

Fabricating Hexagonal Al-Doped $LiCoO_2$ Nanomeshes Based on Crystal-Mismatch Strategy for Ultrafast Lithium Storage

Hai-Tao Xu, Huijuan Zhang, Li Liu, Yangyang Feng, and Yu Wang*

The State Key Laboratory of Mechanical Transmissions and the School of Chemistry and Chemical Engineering, Chongqing University, 174 Shazheng Street, Shapingba District, Chongqing City, P. R. China 400044

Supporting Information

ABSTRACT: In the designed synthesis, low crystal-mismatch strategy has been applied in the synthesis of ion-doped $LiCoO_2$ materials, and a good success of single crystal property has been achieved between the precursor and the final sample for the first time. The hexagonal $LiCo_{0.8}Al_{0.26}O_2$ (LCAO) nanomesh possesses several advantages in morphology and crystal structure, including mesoporous structure, single crystal, atomic even distribution, high exposing surface area as (100) or their equivalent planes, and shortened Li ions diffusion distance. All the merits are beneficial to the application in Li-ion batteries (LIBs) cathode, for example, accelerating Li ions diffusion rate, improving the Li ions shuttle between the LCAO nanomesh and electrolyte, and reducing the Li ions capacitive behavior during Li intercalation. Hence, our research adopts Al-contained precursor with morphology of hexagonal nanoplates to fabricate designed Al-doped $LiCoO_2$ nanomeshes and greatly improves the cathode performance in LIBs.

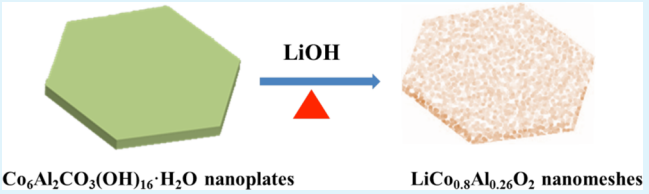

KEYWORDS: *nanomesh, crystal-mismatch, lithium ion battery, hexagonal, Al-doping*

INTRODUCTION

$LiCoO_2$ has long been widely adopted as a commercial cathode material for secondary lithium batteries since the $LiCoO_2$/C system was designed in 1991 by Sony corporation.[1] Since then, Li-ion batteries (LIBs) have significantly attracted much interest in various fields such as satellite phone, transcription machine, laptop computers, etc. Owing to its high energy density, excellent safety, and long cycling life, its application as power source has been extended to industrial application, for instance, electric vehicles (EVs) and hybrid electric vehicles (HEVs). However, $LiCoO_2$ suffers from the high cost of cobalt, which brings serious competition from other materials, such as $LiMn_2O_4$,[2] $LiNiO_2$,[3] and $LiFePO_4$.[4] In the last few decades, many studies have been done to synthesize solid solutions of $LiM_yCo_{1-y}O_2$ (M = Mn, Ni, Mg, Cr, etc.) isostructural with $LiCoO_2$, characterized by low cost, high energy density, excellent cycling ability, and good safety performance.[5−7]

Previously, aluminum had acquired less attention as a solid solution than transition metal elements because it was considered electrochemically inactive due to its fixed valence, giving rise to reduced specific capacity. However, Ceder et al.[8] verified Al as a potentially attractive dopant that could increase the intercalation voltage of $LiCoO_2$. Aydinol and co-workers reported that significant electron transfer to oxygen can occur by the rehybridization of metal−oxygen atomic orbitals, indicating that the conventional views of electron transfer occurring solely between transition metal ions should be revised, and that nontransition metals, including Al, could be considered "electrochemically active".[9] In this regard, many research studies have been carried out on Al-doped $LiCoO_2$. Ohzuku et al.[10] concluded that doping aluminum in transition metal laminate structure is in favor of restraining the anisotropic structural changes, because Al^{3+} along with Li-ions kept the interlayer distance. Jang et al.[11] found that the doping effect of aluminum contributes to preventing the crystal structure of hexagonal $LiCoO_2$ from transformation to spinel during Li-ion extraction and insertion. In conclusion, doping with aluminum has attracted much interest for some merits as follows: (1) Aluminum, compared with cobalt, has the characteristics of low cost and low toxicity. Besides, the density of Al is smaller than that of cobalt, resulting in higher tap density. (2) As verified by Ceder et al.,[8] doping with aluminum contributes to higher lithium-ion intercalation voltage, which is beneficial to improve power density. (3) Doping Al on the layered structure can make for higher lithium diffusivity and lower cycling-induced lattice strain, thanks to the existence of a larger van der Waals gap of the aluminum doping solid solutions and a smaller change in crystal dimension with lithium concentration.[11] (4) As far as we can see, Al^{3+} (r = 0.535 Å) and Co^{3+} (r = 0.545 Å) have similar ionic radii, allowing for a wider scope of solid solution $LiM_yCo_{1-y}O_2$.

Even though Al-doped $LiCoO_2$ had been investigated a couple of years, the designed synthesis of metal ion-doped $LiCoO_2$ materials for high-performance LIBs still remains a great challenge. For example, Myung and co-workers researched the effects of Al doping on the microstructure, but

Received: July 27, 2015
Accepted: September 2, 2015
Published: September 2, 2015

DOI: 10.1021/acsami.5b06844
ACS Appl. Mater. Interfaces 2015, 7, 20979−20986

they did not evaluate in detail the effects on the electrochemical performance.[12] Cho et al.[13] employed Al_2O_3 coating to enhance the structure stability and further improve the capacity of $LiCoO_2$ powder. However, the coating of Al_2O_3 is nonuniform; thus, the cycling ability is not guaranteed. There has been evidence that aluminum-doping $LiCoO_2$ electrode also suffers from serious capacity loss during lithium-ion extraction/insertion, probably arising from the enhanced internal resisitance caused by the rigid structure.[14,15] Besides, the introduction of Al may destroy the continuity of the $LiCoO_2$ crystal. Moreover, in the traditional $LiCoO_2$ materials syntheses, it is very hard to harvest $LiCoO_2$ equal to the fixed molar ratio, especially with uniform morphology and atomic distribution, because in the synthesis the doped elements normally were added in the step of calcinations. As a result, the obtained $LiCoO_2$ materials are irregular and the doped ions are normally unevenly distributed. On the basis of the crystal-mismatch strategy, we used Al-contained precursor with morphology of hexagonal nanoplate to fabricate designed single-crystal Al-doped $LiCoO_2$ nanomeshes; the final sample exhibited several advantages, such as even atomic distribution, uniform morphology, mesoporous structure, and single-crystal feature. More importantly, the electrochemical performance was much better than that of the previously reported results.

As is well-known, $LiCoO_2$ has a layered α-$NaFeO_2$ type structure, providing structure flexibility for introducing lithium ion as a guest species. The capacity of $LiCoO_2$ could reach the maximum of 280 mA·h/g when lithium completely extracts and inserts from the $LiCoO_2$ crystal. Nevertheless, to guard the α-$NaFeO_2$ structure against collapsing, a portion of Li ions is limited to be utilized.[16] Xiao et al. reported that it is favorable for Li^+ to transport along the (010) and (100) planes.[17] By analyzing the ball-and-stick model of LCAO (Figure 1), it is

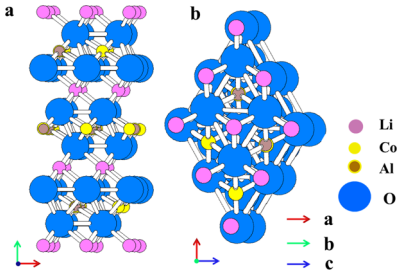

Figure 1. Side views of relaxed (a) {100} or {010} and (b) {001} crystal planes of LCAO to introduce the Li-ion rocking expressway.

obvious that lithium ions could fluently shuttle back and forth in the $LiCoO_2$ crystal along the specific directions, for instance, {100} or {010} . In contrast, we find that it is hard for lithium ions to diffuse the crystal along {001}, because a mass of atoms, such as oxygen or cobalt, obstruct the passing route. On the other hand, to the best of our knowledge, the crystallinity, size of the particles, homogeneity, and morphology mainly govern the electrochemical performance of the $LiAl_yCo_{1-y}O_2$. Considering this observation, it is worthy for us to synthesize designed nanostructured $LiAl_yCo_{1-y}O_2$ with high exposing ratio of (100) or (010) planes, contributing to improved rate capability and cycling ability of $LiAl_yCo_{1-y}O_2$. In our research, involving the low crystal-mismatch tactics, it is the first time that one has obtained the novel Al-doped $LiCoO_2$ with wonderful single crytallinity and mesoporosity simultaneously. As far as we know, no reports have been presented involving the targeted synthesis of Al-doped $LiCoO_2$with architectural properties of mesoporosity and regular morphology. Meanwhile, we compared the electrochemical performance with the presently reported ion-doped $LiCoO_2$ materials, indicating the unique property in the field of energy storage. We have made a big breakthrough in the design and synthesis of $LiCoO_2$ and the application in LIBs cathode, and more importantly we supply a general and simple strategy to fabricate designed single-crystal functional material.

RESULTS AND DISCUSSION

Herein, we report a novel positive electrode material for lithium-ion batteries, Al-doped hexagonal $LiCoO_2$ nanomesh. As far as we know, it has not been presented before. $LiCoO_2$ has been commercialized for a long time, and many researchers believe that there is no need for further studying it. However, by our elaborate analysis of the obtained LCAO, LCAO presents entirely outstanding characteristics in many aspects, such as structure and electrochemical performance. The obtained LCAO has symmetrical hexagonal facets. In addition, the sample possesses the comprehensive characteristics of mesoporosity and single crystallinity. The exposed planes of hexagonal LCAO are indexed as (100) or its equivalent planes. The thickness of the hexagonal nanomesh is limited to 20 nm. Above all, the obtained LCAO delivers a discharge capacity of 188 mA·h g^{-1} at 0.1 C, remarkable cyclability without obvious capacity fading after 200 cycles, and enhanced rate capability of ~137 mA·h g^{-1} at 5 C. All these outstanding results demonstrate that the hexagonal LCAO nanomesh could be the most vigorous competitors in the high-performance LIBs.

To begin with, $Co_6Al_2CO_3(OH)_{16}·H_2O$ precusor was synthesized via a hydrothermal process. Figure 2a is the X-ray diffraction pattern (Co Kα radiation) of the shaped hexagonal Co−Al layered double hydroxides (Co−Al LDHs), which is indexed as the compound of $Co_6Al_2CO_3(OH)_{16}·H_2O$ (JCPDS: 51-0045).[18] The typical peaks of Co−Al LDH are observed and indexed as (003), (006), and (012) planes.[19,20] Figure 2b is the field emission scanning electron microscope (FESEM) image to verify the huge yield of Co−Al LDH. As shown in Figure 2c, Co−Al LDH consists of symmetrical and papery hexagonal nanoplates and the thickness is confined to 20 nm judging by the side view of Co−Al LDH crystal. Furthermore, the magnified FESEM image of the freestanding Co−Al LDH in Figure 2d further confirms that the morphology of Co−Al LDH is shaped hexagonal nanosheet distribution within 200−400 nm. Above all, the obtained Co−Al LDH precursor exhibits significant advantages in many aspects, for instance, structure, size, well distribution, and crystallinity, compared with the conventional coprecipitation method.[21−23]

Figure 3a is the X-ray diffraction pattern (Co Kα radiation) of the calcined product of Co−Al LDH, in which all intense peaks could be well-indexed to hexagonal $LiAl_yCo_{1-y}O_2$ ($0 \le y \le 1$). To verify the existence form of aluminum element, X-ray photoelectron spectroscopy (XPS) analysis was adopted (Supporting Information, Figure S1). As can be seen from the Al 2p spectrum of LCAO nanomesh, a single peak at 73.1 eV is observed. However, according to the previous literature, the Al 2p of Al_2O_3 is located at 74.3 eV.[24,25] The XPS and X-ray diffraction pattern (no peaks for Al_2O_3) results demonstrate the formation of solid solution in LCAO crystal, and the aluminum in precursor is totally transformed into LCAO nanomesh. Figure 3b shows the large-scale FESEM image of LCAO hexagonal crystal, revealing that symmetrical hexagonal shape

DOI: 10.1021/acsami.5b06844
ACS Appl. Mater. Interfaces 2015, 7, 20979−20986

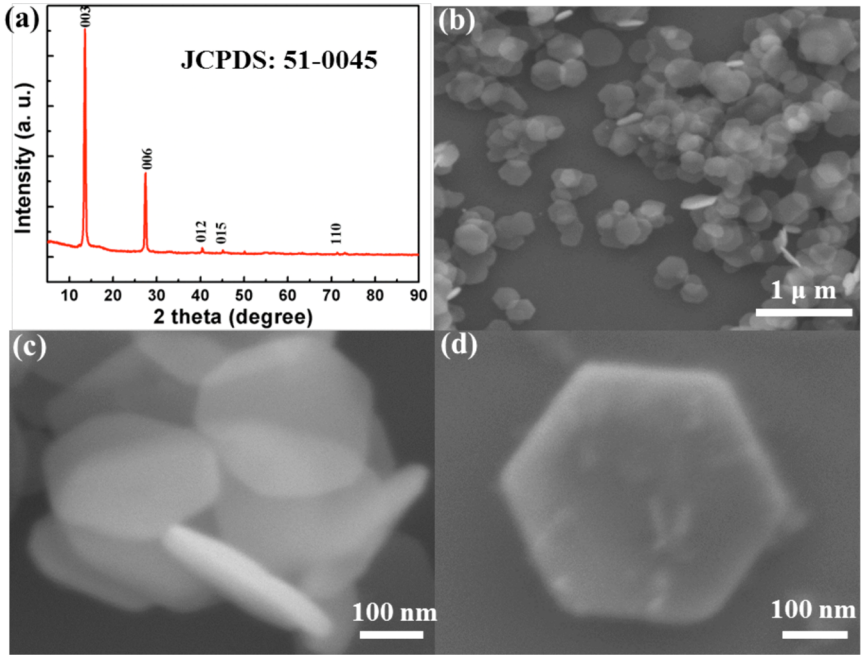

Figure 2. (a) X-ray diffraction (XRD) profile for the $Co_6Al_2CO_3(OH)_{16}·H_2O$ precursor. (b, c) FESEM images of $Co_6Al_2CO_3(OH)_{16}·H_2O$ nanoplates with different magnifications. (d) FESEM image to show the freestanding hexagonal $Co_6Al_2CO_3(OH)_{16}·H_2O$ faceted crystals.

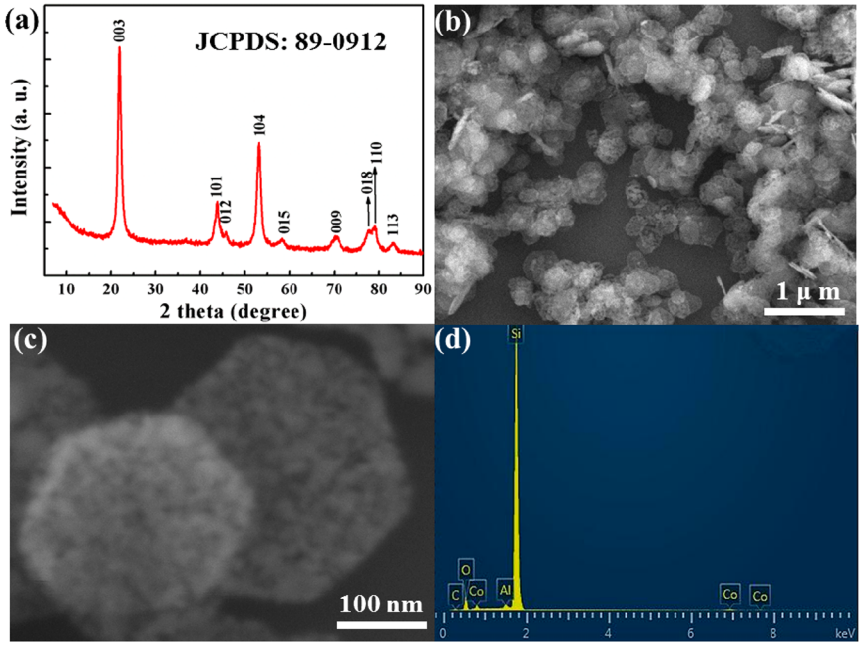

Figure 3. (a) X-ray diffraction (XRD) profile for the LCAO nanomeshes. (b) FESEM image of LCAO nanoplates. (c) FESEM image to show the nanoporous hexagonal LCAO crystals. (d) X-ray energy dispersive spectrum (EDS) is to show the presence of elements in LCAO nanomesh.

of Co−Al LDH has been preserved after calcining at 500 °C. As can be seen in the magnified FESEM image in Figure 3c, the size of the monodisperse shaped hexagonal nanosheet is 200−400 nm, consistent with the Co−Al LDH precursors. Energy-dispersive X-ray (EDX) spectroscopy in Figure 3d confirms the existence of Co, Al, and O in LCAO faceted crystals. To further study the distribution of elements, the elemental distribution spectroscopy mapping in Figure 4 indicates that Co, Al, and O are all well-distributed in the shaped hexagonal nanosheet. In the traditional $LiCoO_2$ materials syntheses, it is very hard to harvest $LiCoO_2$ with fixed doping molar ratio, especially with uniform morphology and even atomic distribution, because in the synthesis normally the doped elements are added in the step of calcinations. However, in our research, the Al-contained precursor was applied and the final sample exhibits several advantages, such as even atomic distribution, uniform morphology, and mesoporous structure. In fact, the $Co_6Al_2CO_3(OH)_{16}·H_2O$ reacts with LiOH at the experimental temperature with release of the gaseous species such as CO_2 and H_2O, which gives rise to the formation of mesopores in the active material.

DOI: 10.1021/acsami.5b06844
ACS Appl. Mater. Interfaces 2015, 7, 20979−20986

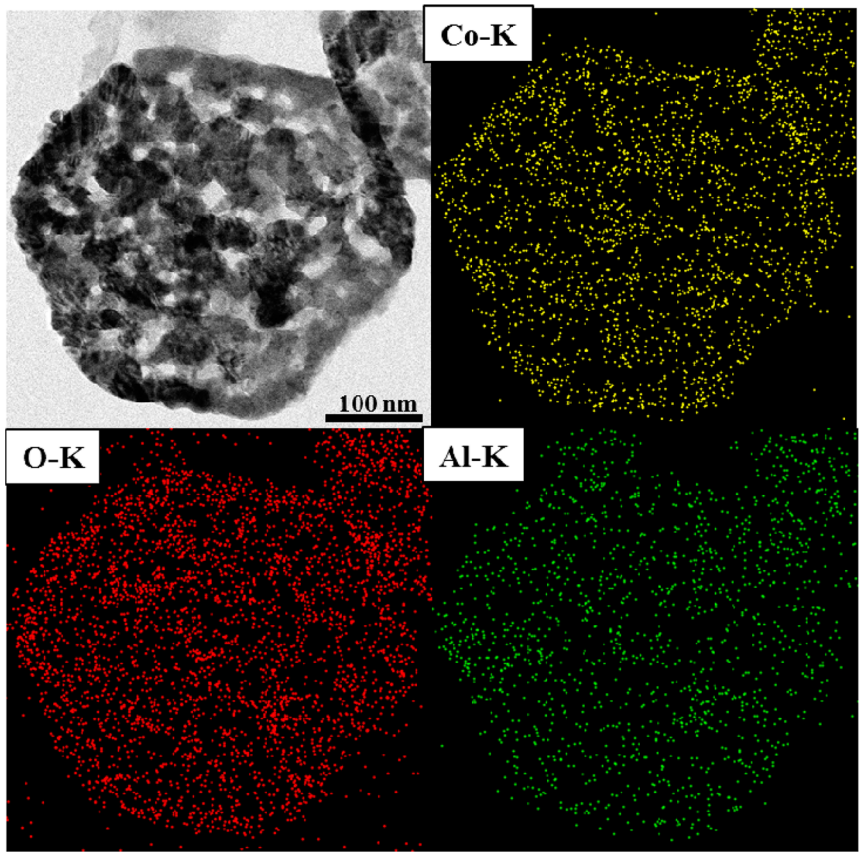

Figure 4. Elemental mapping of LCAO nanomeshes.

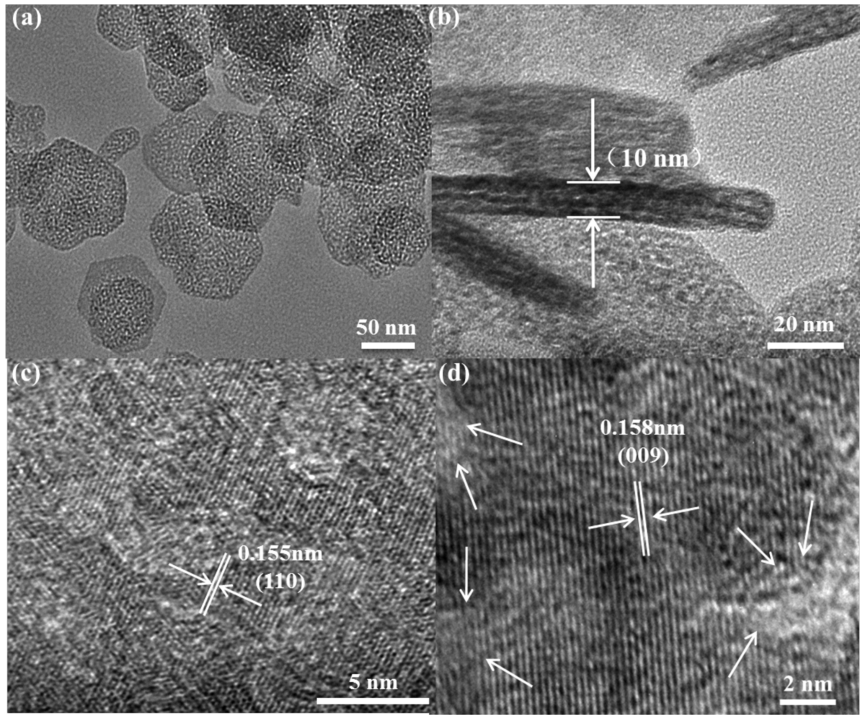

Figure 5. (a) TEM image of faceted LCAO crystal. (b) Side view of a LCAO nanomesh, from which the thickness can be determined. (c, d) HRTEM images of $Co_6Al_2CO_3(OH)_{16}{\cdot}H_2O$ precursor (c) and LCAO nanomesh (d).

Moreover, the crystal structure, morphology, and microstructure of the obtained LCAO are analyzed via transmission electron microscopy (TEM) and high-resolution TEM (HRTEM) analyses. Figure 5a presents a TEM image of monodispersed hexagonal LCAO nanoplates, in which the porous structure are clearly visible. According to the Brunauer–

DOI: 10.1021/acsami.5b06844
ACS Appl. Mater. Interfaces 2015, 7, 20979−20986

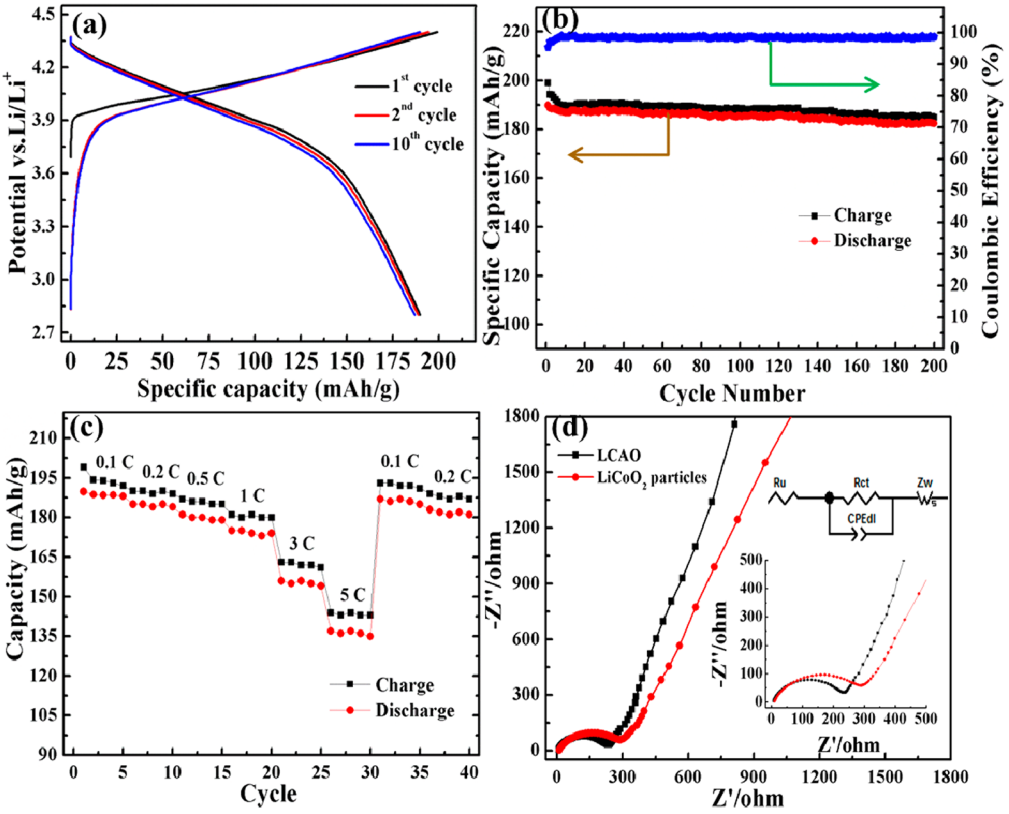

Figure 6. (a) Initial charge−discharge voltage profiles of the LCAO nanomesh at 0.1 C. (b) Cycling performance of the LCAO electrode at 0.1 C. (c) Rate-capability measurement for the LCAO nanomesh. (d) ac impedance spectra of LCAO nanomeshes and $LiCoO_2$ nanoparticles. The inset shows the magnified spectra in low frequency and the equivalent circuit.

Emmett−Teller (BET) analysis (Supporting Information, Figure S2), the surface areas of the product are increased from 48.21 to 84.49 $m^2 \cdot g^{-1}$ during the calcination process and the pore size is also shifted from about 8 to 15 nm. Besides, the Barrett−Joyner−Halenda (BJH) pore-size distribution, shown as the insets of Figure S2b, manifests that the hexagonal LCAO nanomesh possesses regular mesopores, mainly focusing in ∼15 nm. As a result, the large surface area and regular mesopores make it possible for active materials being fully infiltrated into the electrolyte, which is greatly beneficial for Li^+ rapidly shuttling between electrolyte and LCAO nanomesh.[26] The FESEM, TEM, and BET images solidify the mesoporosity feature of hexagonal LCAO nanosheets, providing direct proof to identify the LCAO nanomesh. Figure 5b shows a side view of LCAO crystals, and the thickness could further be judged to be ∼10 nm. In addition, it is visible that the LCAO dominates the stratified structure, constituted by layer upon layer stacking.

As shown in Figure 2d, the Co−Al LDH precursor without using any templates possesses shaped hexagonal symmetry, manifesting that the Co−Al LDH may be single crystal.[27−29] The HRTEM image of precursor (Figure 5c) further certifies the hypothesis of a single-crystalline feature for Co−Al LDH, which exhibits clear and successive crystal lattice with *d*-spacing of 0.155 nm, corresponding to the (110) plane of hexagonal $Co_6Al_2CO_3(OH)_{16}\cdot H_2O$. Meanwhile, from HRTEM image of LCAO nanomesh in Figure 5d, the crystal lattice spacing is measured to be 0.158 nm, in good agreement with the *d*-spacing of (009) facts. It is evident to find that the above lattice spacing is in close proximity to that of (110) in hexagonal Co−Al LDH precursors. In addition, a number of mesopores in the hexagonal LCAO nanomesh are apparently detected in Figure 5d (as marked by white arrows), causing the hexagonal LCAO nanomesh to be divided into several nanocrystal subunits. That is to say, the hexagonally shaped LCAO nanomesh could be considered to be composed of primary nanocrystal subunits sharing the same crystallographic direction along with the longitude and latitude, which certifies that the materials possibly possess the characteristic of the mesocrystal, as reported in previous literature.[30,31] The fabrication tactics rely on the small crystal mismatch of 2% between $Co_6Al_2CO_3(OH)_{16}\cdot H_2O$ and LCAO, further supplying solid proof for the mesocrystal feature of LCAO nanomesh, in which all the building nanocrystal subunits are highly oriented and aligned.[32,33] Besides, electron diffraction (Supporting Information, Figure S3) further verifies the mesocrystal feature of LCAO with single-crystal-like diffraction spots and reveals that the LCAO nanomesh has exposed (001) planes or their equivalent planes.

For the sake of investigating the remarkable electrochemical performance of the LCAO nanomesh, it is necessary to precisely study the charge−discharge curve, cyclic voltammetry (CV), and electrochemical impedance spectroscopy (EIS) profiles. The representative galvanostatic discharge and charge voltage profiles of LCAO nanomesh are displayed in Figure 6a, and the initial discharge capacity of LCAO electrode is 189 mA·h/g at 0.1 C, which precedes those previously reported for Al-doped $LiCoO_2$ powder.[12,14,34] Furthermore, the discharge plateau of LCAO nanomesh is at ∼3.9 V vs Li^+/Li, higher than that of the conventional $LiCoO_2$.[35−39] For instance, Cao et al.[37] reported that the PPy-coated $LiCoO_2$ exhibited an initial discharge capacity of 182 mA·h/g and maintained 94.3% after170 cycles, which indicates the Al-doped $LiCoO_2$ nano-

DOI: 10.1021/acsami.5b06844
ACS Appl. Mater. Interfaces 2015, 7, 20979−20986

meshes possess high capacity and Coulombic efficiency. Meanwhile, the LCAO achieve a voltage plateau at 4.08 V in the charge process. For the sake of confirming the reliability of the results, cyclic voltammetry tests were carried out to examine the charge and discharge process in Supporting Information, Figure S4. The CV curve indicates that LCAO has a pair of cathodic peaks at 3.9 V and an anodic peak at 4.08 V, demonstrating that the Al-doped $LiCoO_2$ nanomesh possesses higher power density. Besides, as seen in Figure S4, the curves are nearly overlapped during the three cycles, demonstrating the excellent reversibility of the LCAO electrode. For testing the cycling life of LCAO nanomesh, ultralong charge and discharge cycling at 0.1 C (1 C is equal to 280 mA·h/g) is conducted and shown in Figure 6b, exhibiting an ultrahigh Coulombic efficiency with an average value of 98.7% during 200 cycles. After 200 cycles, LCAO nanomesh still delivers a reversible capacity of 183 mA·h/g (equal to 96.8% capacity retention), manifesting outstanding cycling ability at low current rate due to the effect of Al doping. By carefully observing the LCAO electrode at 0.1 C after 200 cycles (Supporting Information, Figure S5), we found that the LCAO crystal still maintained the shaped hexagonal as well as good crystallinity, which provides solid support for the outstanding cycling ability. According to the previous literature reported,[12,14] as the Li-ion deintercalation/intercalation in Al-doped $LiCoO_2$ crystal, the *a*-axis is shrunken and the *c*-axis is amplified, providing more extensive diffusion pathways for Li-ion. Figure 6c is the rate performance of the LCAO nanomesh at different current rates. As seen in Figure 6c, the capacity is within the range of 189−137 mA·h g^{-1} at various current densities from 0.1 to 5 C. Remarkably, an ultrahigh reversible capacity of 137 mA·h g^{-1} could be maintained even at the maximum investigated current density of 5 C. In general, the Li insertion and extraction comply with a two-phase Li diffusion-limited transfer process and finally lead to a reversible capacity loss with the increasing current densities.[40] More importantly, when the current density returns to the original current density, the specific capacity could be nearly recovered to 185 mA·h g^{-1}, manifesting the greatly improved rate ability and cyclability of the hexagonal LCAO nanomesh. Normally $LiCoO_2$ electrodes exhibit high specific capacities instead of good rate ability.[41,42] However, the mesporous LCAO crystal is exempt from varying discharge and charge densities, making it preferred for high power applications. For investigating further kinetic details of the LCAO nanomesh, electrochemical impedance experiments were conducted and are shown in Figure 6d. The $LiCoO_2$ particles were prepared via the method reported by Ying et al.[43] According to the AC impedance measurements results of the samples (Supporting Information, Table S1), the charge-transfer resistance (R_{ct}) of LCAO nanomeshes (220.4 Ω) is smaller than that of $LiCoO_2$ particles (325.1 Ω). Besides, the R_{SEI} in the $LiCoO_2$ particles is ∼2 times as large as that of LCAO nanomeshes, 14.42 Ω versus 7.47 Ω. The electrochemical impedance spectroscopy (EIS) result demonstrates that not only the charge-transfer resistance but also the SEI resistance are debased in LCAO nanomesh. In a word, the hexagonal single-crystal LCAO nanomesh manifests excellent electrochemical performance, compared to the reported $LiCoO_2$ (Supporting Information, Table S2). The findings mentioned in this work verify that structural and morphological novelty as well as the Al-doping effect of the $LiCoO_2$ nanomesh play a significant part in its commercialization in Li-ion battery cathode, for example, portable electronic devices, hybrid electric vehicles, and grid energy storage. In this research, hexagonal single-crystal Al-doped $LiCoO_2$ nanomesh has huge exposed ratio planes indexed as (100) or their equivalent planes and simultaneously shrinks the longitude dimension to ∼10 nm along the Li rapid diffusion direction. Additionally, the hexagonal LCAO possesses a mesoporosity feature, making it easier for the electrolyte to fluently shuttle between electrode materials. In general, the above-mentioned features contribute to generating high-performance electrode materials for lithium-ion batteries, which have a highly reversible specific capacity, good rate ability, and remarkable cyclability.

CONCLUSION

In conclusion, a novel hexagonal single-crystal LCAO nanomesh has been designed and synthesized with the guidance of a low crystal-mismatch strategy for the first time. Compared with a traditional $LiCoO_2$ nanoparticle, the Al-doped $LiCoO_2$ nanomesh not only improves the voltage platform but also cuts down the cost. More remarkably, the lithium-ion rapid diffusion planes of (100) or their equivalent planes have tremendous exposing ratio near the 100% ratio, which remarkably improves the cyclability and rate ability of LCAO. Furthermore, the nanomesh's longitude dimension is confined within 10 nm. Meanwhile, the unique nanomesh delivers synergistic features of mesoporosity and single crystal. All the virtues mentioned empower the LCAO nanomesh with a significantly improved electrochemical performance for positive electrode materials, concerning the high specific capacity, eminent rate capability, remarkable cycling ability, and attractive Coulombic efficiency, qualifying it as a promising electrode material candidate for advanced Li-ion batteries.

EXPERIMENTAL SECTION

Materials. All chemicals or materials were used directly without any further purification before use: ethylene glycol (Fisher Chemical, 99.99%), aluminum nitrate ($Al(NO_3)_3$, 99.9%, Aldrich), cobalt nitrate ($Co(NO_3)_2$, 99.9%, Aldrich), ammonium hydroxide ($NH_3{\cdot}H_2O$, 28−30 wt %), Sodium carbonate (Na_2CO_3, 99.9%, Aldrich), and metallic Li foil (99.9%, Aldrich).

Preparation of $Co_6Al_2CO_3(OH)_{16}{\cdot}H_2O$ Nanoplates. In a typical synthesis of $Co_6Al_2CO_3(OH)_{16}{\cdot}H_2O$ nanoplates, ethylene glycol (14.5 mL), ammonium hydroxide (12.5 mL), 1 M Na_2CO_3 aqueous solution (5 mL), 1 M $Co(NO_3)_2$ aqueous solution (5 mL), and 1 M $Al(NO_3)_3$ aqueous solution (2 mL) were mixed step by step under violent stirring with intervals of 1 min. The solutions were stirred for another 10 min, accompanied by the color of the solution turning pink. Afterward, the resulting solution was transferred into a 45 mL Teflon autoclave, followed by a thermal treatment process at 180 °C for 18 h in the traditional oven. Then the autoclave was transferred into the fuming cupboard for cooling down to room temperature; the precipitate on the bottom was gathered and washed by centrifuging for at least three cycles using deionized water and three cycles using pure ethanol. The obtained samples were then dried in a vacuum oven at 60 °C for a night so as to remove the absorbed water and ethanol for the subsequent characterizations.

Preparation of $LiCo_{0.8}Al_{0.26}O_2$ Nanomeshes. $Co_6Al_2CO_3(OH)_{16}{\cdot}H_2O$ nanoplates were evenly mixed with LiOH powder in a molar ratio of 1:7.5 under the aid of ethanol. Then the mixtures were calcined at 500 °C for 200 min in air atmosphere.

Characterization of the Samples. Field emission scanning electron microscope (FESEM, JEOL, JSM-7800F, 1−30 kV), transmission electron microscopy (TEM, Philips, Tecnai, F30, 300 kV) coupled with EDS analyzer, powder X-ray diffraction (XRD, Bruker D8 Advance X-ray diffractometer with Co Kα radiation), inductively coupled plasma-atomic emission spectroscopy (ICP-AES, iCAP6300 Duo), and Brunauer−Emmett−Teller surface area

DOI: 10.1021/acsami.5b06844
ACS Appl. Mater. Interfaces 2015, 7, 20979−20986

measurement (BET, Quantachrome Autosorb-6B surface area and pore size analyzer) were adopted to characterize the as-prepared samples.

Electrochemical Characterization. For electrochemical tests, a homogeneous mixture composed of active material, carbon black, and polyvinyl difluoride (PVDF) using 1-methyl-2-pyrrolidinone (NMP) as solvent in weight ratio of 80:10:10 was prepared under strong magnetic stirring for at least 1 day. The slurry was then extracted and spread on to aluminum foil. Prior to cell fabrication, the electrodes were heated in a vacuum oven at 120 °C for 8 h. The electrolyte was 1 M $LiPF_6$ dissolved in a compound of ethylene carbonate (EC) and diethyl carbonate (DEC) with a 1:1 volume ratio, and the separator was a microporous polypropylene film (Celgard 2400). Lithium metal (99.9%, Aldrich) was adopted as a counter electrode. The cell was assembled in a glovebox filled with high-purity argon gas. Besides, the cathode loading was 2 mg/cm^2. The electrochemical performance of LCAO electrode was tested via a battery testing system at different rates in the range of 2.8−4.3 V. Cyclic voltammetry and electrochemical impedance spectroscopy measurements of the cells were made using the three-electrode system on electrochemical working station CHI660D. For the EIS measurements, the frequency range was between 100 kHz and 10 mHz.

■ ASSOCIATED CONTENT

Supporting Information

The Supporting Information is available free of charge on the ACS Publications website at DOI: 10.1021/acsami.5b06844.

More SEM, BET image, and electrochemical testing data (PDF)

■ AUTHOR INFORMATION

Corresponding Author

*E-mail: wangy@cqu.edu.cn; prospectwy@gmail.com.

Notes

The authors declare no competing financial interest.

■ ACKNOWLEDGMENTS

This work was financially supported by the Thousand Young Talents Program of the Chinese Central Government (Grant no. 0220002102003), National Natural Science Foundation of China (NSFC, Grant no. 21373280, 21403019), the Fundamental Research Funds for the Central Universities (0301005202017), Beijing National Laboratory for Molecular Sciences (BNLMS), and Hundred Talents Program at Chongqing University (Grant no. 0903005203205).

■ REFERENCES

(1) Ozawa, K. Lithium-Ion Rechargeable Batteries with $LiCoO_2$ and Carbon Electrodes: The $LiCoO_2$/C System. *Solid State Ionics* **1994**, *69*, 212−221.

(2) Manev, V.; Banov, B.; Momchilov, A.; Nassalevska, A. $LiMn_2O_4$ for 4 V Lithium-Ion Batteries. *J. Power Sources* **1995**, *57*, 99−103.

(3) Li, W.; Currie, J. C.; Wolstenholme, J. Influence of Morphology on the Stability of $LiNiO_2$. *J. Power Sources* **1997**, *68*, 565−569.

(4) Padhi, A. K.; Nanjundaswamy, K. S.; Goodenough, J. B. Phospho-olivines as Positive-Electrode Materials for Rechargeable Lithium Batteries. *J. Electrochem. Soc.* **1997**, *144*, 1188−1194.

(5) Stoyanova, R.; Zhecheva, E.; Zarkova, L. Effect of Mn-Substitution for Co on the Crystal Structure and Acid Delithiation of $LiMn_yCo_{1-y}O_2$ Solid Solutions. *Solid State Ionics* **1994**, *73*, 233−240.

(6) Ueda, A.; Ohzuku, T. Solid State Redox Reactions of $LiNi_{1/2}Co_{1/2}O_2$ (R $\bar{3}$m) for 4 V Secondary Lithium Cells. *J. Electrochem. Soc.* **1994**, *141*, 2010−2014.

(7) Yoon, W.-S.; Lee, K.-K.; Kim, K.-B. Structural and Electrochemical Properties of $LiAl_yCo_{1-y}O_2$ Cathode for Li Rechargeable Batteries. *J. Electrochem. Soc.* **2000**, *14*, 2023−2028.

(8) Ceder, G.; Chiang, Y. M.; Sadoway, D. R.; Aydinol, M. K.; Jang, Y. I.; Huang, B. Identification of Cathode Materials for Lithium Batteries Guided by First-Principles Calculations. *Nature* **1998**, *392*, 694−696.

(9) Aydinol, M. K.; Kohan, A. F.; Ceder, G.; Cho, K.; Joannopoulos, J. Ab Initio Study of Lithium Intercalation in Metal Oxides and Metal Dichalcogenides. *Phys. Rev. B: Condens. Matter Mater. Phys.* **1997**, *56*, 1354−1365.

(10) Ohzuku, T.; Ueda, A.; Kouguchi, M. Synthesis and Characterization of $LiAl_{1/4}Ni_{3/4}$ O_2 (R $\bar{3}$m) for Lithium Ion (Shuttlecock) Batteries. *J. Electrochem. Soc.* **1995**, *142*, 4033−4039.

(11) Jang, Y.-I.; Huang, B.; Wang, H.; Sadoway, D. R.; Ceder, G.; Chiang, Y.-M.; Liu, H.; Tamura, H. $LiAl_y$ Co_{1-y} O_2 (R $\bar{3}$m) Intercalation Cathode for Rechargeable Lithium Batteries. *J. Electrochem. Soc.* **1999**, *146*, 862−868.

(12) Myung, S.-T.; Kumagai, N.; Komaba, S.; Chung, H.-T. Effects of Al Doping on the Microstructure of $LiCoO_2$ Cathode Materials. *Solid State Ionics* **2001**, *139*, 47−56.

(13) Cho, J.; Kim, Y. J.; Park, B. Novel $LiCoO_2$ Cathode Material with Al_2O_3 Coating for a Li Ion Cell. *Chem. Mater.* **2000**, *12*, 3788−3791.

(14) Goldberger, J.; He, R.; Zhang, Y.; Lee, S.; Yan, H.; Choi, H.-J.; Yang, P. Single-Crystal Gallium Nitride Nanotubes. *Nature* **2003**, *422*, 599−602.

(15) Castro-García, S.; Castro-Couceiro, A.; Señarís-Rodríguez, M. A.; Soulette, F.; Julien, C. Influence of Aluminum Doping on the Properties of $LiCoO_2$ and $LiNi_{0.5}Co_{0.5}O_2$ Oxides. *Solid State Ionics* **2003**, *156*, 15−26.

(16) Wang, D. S.; Ma, X. L.; Wang, Y. G.; Wang, L.; Wang, Z. Y.; Zheng, W.; He, X. M.; Li, J.; Peng, Q.; Li, Y. D. Shape Control of CoO and $LiCoO_2$ Nanocrystals. *Nano Res.* **2010**, *3*, 1−7.

(17) Xiao, X. L.; Liu, X. F.; Wang, L.; Zhao, H.; Hu, Z. B.; He, X. M.; Li, Y. D. $LiCoO_2$ Nanoplates with Exposed (001) Planes and High Rate Capability for Lithium-Ion Batteries. *Nano Res.* **2012**, *5*, 395−401.

(18) Liu, Z. P.; Ma, R. Z.; Osada, M.; Iyi, N.; Ebina, Y.; Takada, K.; Sasaki, T. Synthesis, Anion Exchange, and Delamination of Co−Al Layered Double Hydroxide: Assembly of the Exfoliated Nanosheet/Polyanion Composite Films and Magneto-optical Studies. *J. Am. Chem. Soc.* **2006**, *128*, 4872−4880.

(19) Su, L.-H.; Zhang, X.-G.; Liu, Y. Electrochemical Performance of Co−Al Layered Double Hydroxide Nanosheets Mixed with Multiwall Carbon Nanotubes. *J. Solid State Electrochem.* **2008**, *12*, 1129−1134.

(20) Xue, R.; Sun, Z.; Su, L.; Zhang, X. Large-Scale Synthesis of Nitrogen-Doped Carbon Nanotubes by Chemical Vapor Deposition Using a Co-Based Catalyst from Layered Double Hydroxides. *Catal. Lett.* **2010**, *135*, 312−320.

(21) Li, F.; Duan, X. Applications of Layered Double Hydroxides. In *Layered Double Hydroxides*; Duan, X., Evans, D., Eds.; Springer: Berlin/Heidelberg, 2006; Chapter 7, pp 193−223.

(22) Peng, D. F.; Beysen, S.; Li, Q. A.; Sun, Y. F.; Yang, L. Y. Hydrothermal Synthesis of Monodisperse Alpha-Fe_2O_3 Hexagonal Platelets. *Particuology* **2010**, *8*, 386−389.

(23) Kuang, Y.; Zhao, L. N.; Zhang, S. A.; Zhang, F. Z.; Dong, M. D.; Xu, S. L. Morphologies, Preparations and Applications of Layered Double Hydroxide Micro-/Nanostructures. *Materials* **2010**, *3*, 5220−5235.

(24) Lopez, S.; Petit, J.-P.; Tourillon, G.; Dunlop, H. M.; Butruille, J.-R. Acid−Base Properties of Passive Films on Aluminum: II. An X-ray Photoelectron Spectroscopy and X-ray Absorption Near Edge Structure Study. *J. Electrochem. Soc.* **1998**, *145*, 829−834.

(25) Alexander, M. R.; Beamson, G.; Bailey, P.; Noakes, T. C. Q.; Skeldon, P.; Thompson, G. E. The Distribution of Hydroxyl Ions at the Surface of Anodic Alumina. *Surf. Interface Anal.* **2003**, *35*, 649−657.

DOI: 10.1021/acsami.5b06844
ACS Appl. Mater. Interfaces 2015, 7, 20979−20986

(26) Bruce, P. G.; Scrosati, B.; Tarascon, J. M. Nanomaterials for Rechargeable Lithium Batteries. *Angew. Chem., Int. Ed.* **2008**, *47*, 2930−2946.
(27) Bauerlein, E. Biomineralization of Unicellular Organisms: An Unusual Membrane Biochemistry for the Production of Inorganic Nano- and Microstructures. *Angew. Chem., Int. Ed.* **2003**, *42*, 614−641.
(28) Aizenberg, J.; Muller, D. A.; Grazul, J. L.; Hamann, D. R. Direct Fabrication of Large Micropatterned Single Crystals. *Science* **2003**, *299*, 1205−1208.
(29) Yang, S.; Yang, B. X.; Wu, L.; Li, Y. H.; Liu, P. R.; Zhao, H. J.; Yu, Y. Y.; Gong, X. Q.; Yang, H. G. Titania Single Crystals with a Curved Surface. *Nat. Commun.* **2014**, *5*, 5355−5361.
(30) Xu, A. W.; Antonietti, M.; Colfen, H.; Fang, Y. P. Uniform Hexagonal Plates of Vaterite $CaCO_3$ Mesocrystals Formed by Biomimetic Mineralization. *Adv. Funct. Mater.* **2006**, *16*, 903−908.
(31) Liu, Z.; Wen, X. D.; Wu, X. L.; Gao, Y. J.; Chen, H. J.; Zhu, J.; Chu, P. K. Intrinsic Dipole-Field-Driven Mesoscale Crystallization of Core−Shell ZnO Mesocrystal Microsphere. *J. Am. Chem. Soc.* **2009**, *131*, 9405−9412.
(32) Zhang, H. J.; Wong, C. C.; Wang, Y. Crystal Engineering of Nanomaterials To Widen the Lithium Ion Rocking "Express Way": A Case in $LiCoO_2$. *Cryst. Growth Des.* **2012**, *12*, 5629−5634.
(33) Wang, Y.; Zhang, H. J.; Wei, J.; Wong, C. C.; Lin, J.; Borgna, A. Crystal-Match Guided Formation of Single-Crystal Tricobalt Tetraoxygen Nanomesh as Superior Anode for Electrochemical Energy Storage. *Energy Environ. Sci.* **2011**, *4*, 1845−1854.
(34) Jones, C. D. W.; Rossen, E.; Dahn, J. R. Structure and Electrochemistry of $Li_xCryCo_{1-y}O_2$. *Solid State Ionics* **1994**, *68*, 65−69.
(35) Chen, H. L.; Grey, C. P. Molten Salt Synthesis and High Rate Performance of the "Desert-Rose" Form of $LiCoO_2$. *Adv. Mater.* **2008**, *20*, 2206−2210.
(36) Okubo, M.; Hosono, E.; Kim, J.; Enomoto, M.; Kojima, N.; Kudo, T.; Zhou, H. S.; Honma, I. Nanosize Effect on High-Rate Li-Ion Intercalation in $LiCoO_2$ Electrode. *J. Am. Chem. Soc.* **2007**, *129*, 7444−7452.
(37) Cao, J. C.; Hu, G. R.; Peng, Z. D.; Du, K.; Cao, Y. B. Polypyrrole-Coated $LiCoO_2$ Nanocomposite with Enhanced Electrochemical Properties at High Voltage for Lithium-Ion Batteries. *J. Power Sources* **2015**, *281*, 49−55.
(38) Wang, Z. G.; Wang, Z. X.; Guo, H. J.; Peng, W. J.; Li, X. H. Improving the Cycling Stability of $LiCoO_2$ at 4.5 V through Co-modification by Mg Doping and Zirconium Oxyfluoride Coating. *Ceram. Int.* **2015**, *41*, 469−474.
(39) Liu, L.; Chen, J. D.; Bai, Y. J.; Fang, L.; Zhang, H. J.; Wang, Y. Designed Synthesis of $LiFe_{0.2}Co_{0.8}O_2$ Nanomeshes to Greatly Improve the Positive Performance in Lithium-Ion Batteries. *J. Mater. Chem. A* **2015**, *3*, 6671−6678.
(40) Delacourt, C.; Poizot, P.; Tarascon, J.-M.; Masquelier, C. The Existence of a Temperature-Driven Solid Solution in Li_xFePO_4 for $0 \leq x \leq 1$. *Nat. Mater.* **2005**, *4*, 254−260.
(41) He, P.; Wang, H. R.; Qi, L.; Osaka, T. Synthetic Optimization of Spherical $LiCoO_2$ and Precursor via Uniform-Phase Precipitation. *J. Power Sources* **2006**, *158*, 529−534.
(42) Wei, T.; Zeng, R.; Sun, Y. M.; Huang, Y. H.; Huang, K. V. A Reversible and Stable Flake-like $LiCoO_2$ Cathode for Lithium Ion Batteries. *Chem. Commun.* **2014**, *50*, 1962−1964.
(43) Ying, J. R.; Jiang, C. Y.; Wan, C. R. Preparation and Characterization of High-Density Spherical $LiCoO_2$ Cathode Material for Lithium Ion Batteries. *J. Power Sources* **2004**, *129*, 264−269.

DOI: 10.1021/acsami.5b06844
ACS Appl. Mater. Interfaces 2015, 7, 20979−20986